Supporting Information for

Climatic impact of Arctic Ocean methane hydrate dissociation in the 21st-century

Sunil Vadakkepuliyambatta[1*], Ragnhild B Skeie[2], Gunnar Myhre[2], Stig B Dalsøren[2], Anna Silyakova[1], Norbert Schmidbauer[3], Cathrine Lund Myhre[3], Jürgen Mienert[1]

[1]CAGE-Center for Arctic Gas Hydrate, Environment and Climate, Department of Geosciences, UiT-The Arctic University of Norway, 9037 Tromsø, Norway.

[2]CICERO-Center for International Climate and Environmental Research – Oslo, PB. 1129 Blindern, 0318 Oslo, Norway.

[3]NILU - Norwegian Institute for Air Research, Instituttveien 18, 2027 Kjeller, Norway.

.

Contents of this file

Text S1 to S5
Figures S1 to S5
Tables S1 to S2

Text S1 Input for present-day estimation the gas hydrate inventory

The area of the Arctic Ocean north of 65° latitude is considered for quantifying the gas hydrates. The input data used for this estimation is listed below.

Bathymetry: We use the IBCAO v3 bathymetric grid [*Jakobsson et al.*, 2012]. It has a resolution of ~500x500 m.

Bottom water temperature: The bottom water temperature data used for the present-day hydrate modeling are extracted from NOAA-NODC World Ocean Database 2013 (https://www.nodc.noaa.gov/OC5/WOD/pr_wod.html). The data were quality-controlled, eliminating water temperature measurements which are from more than 25 m shallower than the water depth at a particular location by comparing it with the bathymetry. The measurements are sparse in the deeper part of the Arctic Ocean (Fig.S1). The data were gridded to a resolution of 30x30 km which were then resampled to 5x5 km.

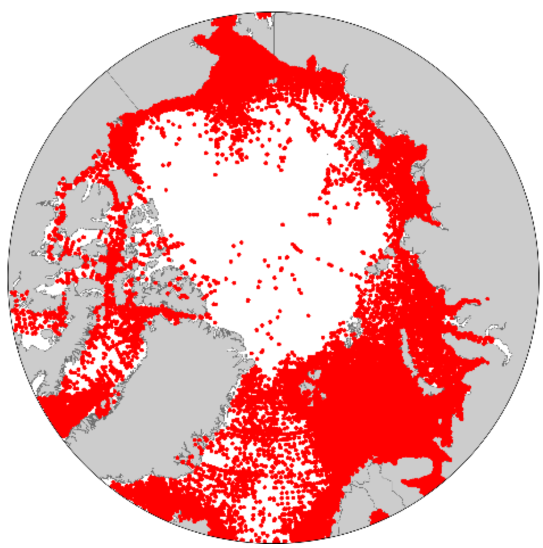

Figure S1. *Distribution of CTD measurements used for the study*

Geothermal gradient: Heat flow measurements in the Arctic (Fig.S2) are used estimating the temperature distribution within the sediments. The available measurements of heat flow are compiled from Global Heat Flow Database (http://www.heatflow.und.edu/index2.html) [*Pollack* *et al.*, 1993] and other published data [*Bugge et al.*, 2002; *Phrampus et al.*, 2014] [BGR cruise report, 2013]. Most of the measurements are made using 5-6 m long steel rods attached with thermal sensors. *Phrampus et al.* [2014] estimate the heat flow from bottom simulating reflections (BSRs) in deep water settings. In addition, thermal conductivity values were also extracted from Global Heat Flow Database wherever available.

Figure S2. *Distribution of heat flow measurements used for the study*

Porosity and hydrate saturation in sediments: The porosity values used for hydrate quantification were obtained from deep ocean drilling data available in the study area (Fig.S3). The porosity values were averaged at every 5 m interval for all the available drill holes, resulting in a mean porosity curve with depth (Fig. S4). The hydrate saturations were obtained from analysis of seismic data conducted in the Western Svalbard region [*Westbrook et al.*, 2008; *Hustoft et al.*, 2009; *Chabert et al.*, 2011]. Their estimated hydrate saturation values fell in the range of 6-12 % of pore space.

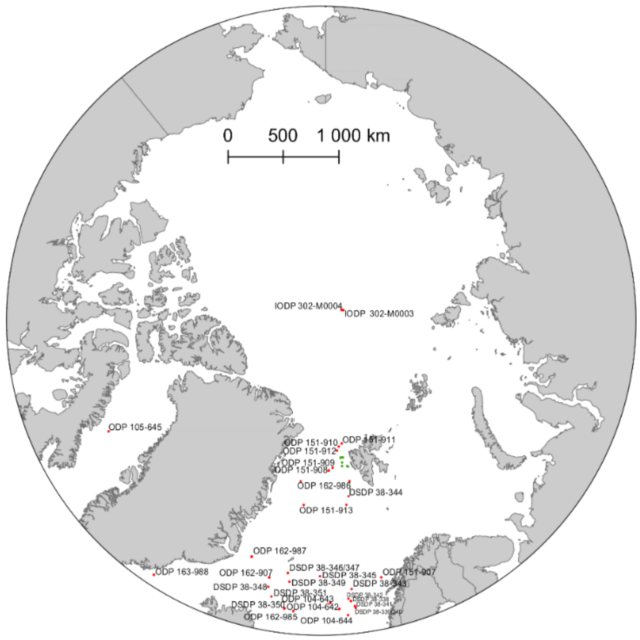

Figure S3. *Location of ODP holes (red dots) and hydrate saturation measurements used in the study.*

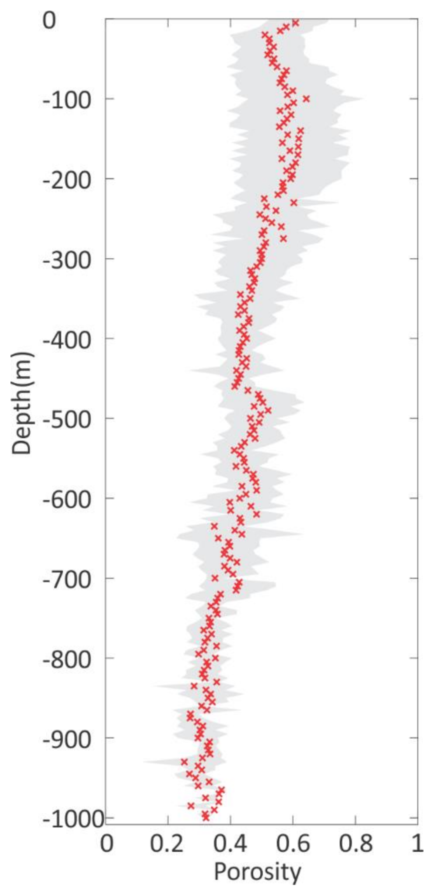

Figure S4. *Porosity curve with depth-averaged from the ODP drill-sites in the Arctic (location on S3). The grey-shaded region represents the uncertainty in porosity at each depth.*

Text S2 Uncertainties related to present-day hydrate quantification

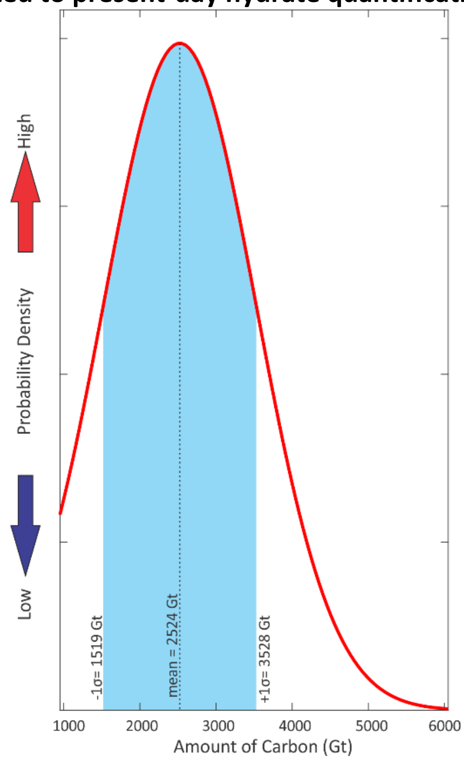

Figure S5. *Probability distribution from a Monte-Carlo style analysis of the uncertainties in the parameters used for quantifying gas hydrates in the marine sediments.*

The impact of uncertainties related to the field observations of various parameters such as thermal gradient, porosity and hydrate saturation on the volume of gas hydrates is analyzed using a Monte-Carlo simulation approach. The observed uncertainties as detailed in S1 are used for hydrate saturation and porosity, whereas a general uncertainty of $\pm$ 10 ^{o}C km^{-1} is applied for the thermal gradient values, based on the maximum uncertainties observed on the West Svalbard margin. The uncertainty analysis suggests that a mean carbon inventory of 2524 $\pm$ 1005 Gt.

Text S3 Climate models

Historical and future seafloor temperature in the Arctic is calculated from nine climate models (Table 1) participating in the fifth phase of the Climate Model Intercomparison Project (CMIP5) [*Taylor et al.*, 2012] . For future climate change (2006-2100), model simulations forced by the RCP 8.5 scenario [*Riahi et al.*, 2011] is used. The annual mean in-situ temperature at the sea floor in the Arctic is calculated based on the model output of potential temperature and salinity. The original model grids were regridded to a 1 x 1 degree grid. This grid is then resampled to 5 x 5 km resolution for 3D diffusive heat flow modeling.

Table S1. *CMIP5 Models used in this study (only the first member of the submitted ensemble of experiments are used).*

Model	Modeling Center	Reference
CanESM2	Canadian Center for Climate Modelling and Analysis	[*Arora et al.*, 2011; *von Salzen et al.*, 2013]
CCSM4	NCAR, US	[*Gent et al.*, 2011]
CESM1(CAM5)	NSF-DOE-NCAR, US	[*Hurrell et al.*, 2013]
GFDL-ESM2M	NOAA GFDL, US	[*Dunne et al.*, 2012; *Dunne et al.*, 2013]
GISS-E2-R	NASA GISS, US	[*Schmidt et al.*, 2006; *Schmidt et al.*, 2014]
HadGEM2-ES	Met Office Hadley Center, UK	[*Collins et al.*, 2011; *Martin et al.*, 2011]
IPSL-CM5A-LR	Institut Pierre Simon Laplace, France	[*Dufresne et al.*, 2013]
MIROC-ESM	University of Tokyo, National Institute for Environmental Studies, and Japan Agency for Marine-Earth Science and Technology	[*Watanabe et al.*, 2011]
MPI-ESM-MR	Max Planck Institute for Meteorology, Germany	[*Jungclaus et al.*, 2013; *Stevens et al.*, 2013]

Text S4 3D Diffusive heat flow modeling

Based on the variations in bottom water temperature from nine future climate models (2006-2100), the conductive transport of heat through marine sediments was estimated using the Fourier's law of heat conduction. It states that the heat flow (q) per unit area and per unit time, at a point in the medium is directly proportional to the temperature gradient at the point [*Turcotte and Schubert*, 2002], which can be expressed mathematically in three dimensions as;

$$q = -k[\frac{dT}{dx} + \frac{dT}{dy} + \frac{dT}{dz}] \quad (1)$$

where T is the temperature, k is the co-efficient of thermal conductivity, and dT/dz is the thermal gradient. The minus sign in equation 1 represents the direction of heat flow from higher temperature to lower temperature.

From equation 1, the general differential equation for rate of heat diffusion with time in three dimensions in a non-deforming medium with constant diffusivity (K) can be written as [*Spiegelman*, 2004; *Gerya*, 2010],

$$\frac{\partial T}{\partial t} = K\left(\frac{\partial^2 T}{\partial x^2} + \frac{\partial^2 T}{\partial y^2} + \frac{\partial^2 T}{\partial z^2}\right) \tag{2}$$

where ∂ is the partial derivative, T is the temperature, t is time, x, y, and z are the coordinates in each direction. ∂T/∂t is the rate of change of temperature with time and ∂T/∂x is the rate of change of temperature in the x-direction.

The diffusivity (K) at each location is estimated as the ratio of thermal conductivity (k) of the sediments and product of density and specific heat capacity of sediments. Thermal conductivities and thermal gradients for the Arctic sediments are taken from the International Heat Flow Commission's World Heat Flow Database [*Pollack et al.*, 1993]. A constant density of 1800 kg m^{-3} and a constant specific heat capacity of 1000 J kg^{-1} K^{-1} are assumed for the entire Arctic sediments.

For each location in the Arctic north of 65^0 N latitude, equation 2 is solved numerically, using a finite-difference technique, assuming no in-situ generation of heat, where the space derivatives are approximated and expanded to second order [*Spiegelman*, 2004; *Gerya*, 2010; *Phrampus and Hornbach*, 2012]. The heat changes due to hydrate formation and dissociation are discounted in the model.

Based on the seafloor temperatures from 2006, geothermal gradients, bathymetry and assuming a linear temperature gradient, a 594 x 594 x 200 cell initial temperature cube is generated (5km x 5km x 5 m cell dimensions) with an upper boundary at the seafloor and basal boundary 1000m below the seafloor. The side boundaries are kept open throughout the model run, whereas the bottom boundary is closed and bottom water temperature is varied at the top boundary. Assuming no significant in situ generation of heat, the 3D finite-difference heat flow model is run explicitly for the period 2006-2100 with time step estimated as $dz^2/(4*K)$. The same process is repeated for seafloor temperatures from all nine climate models.

Text S5 Measurement of methane gas concentrations in the water column

Table S2: *Dissolved methane gas concentration measurements in the Arctic*

Water Depth (m)	Average bottom concentration (nmol l^{-1})	Average surface concentration (nmol l^{-1})	Surface conc. as a percentage of bottom concentration	Area	Month	Reference
45	391	33	8.44	Central North Sea	7	[*Mau et al.*, 2015]
45	600	20	3.33	Central North Sea	1	[*Mau et al.*, 2015]
50	600	10	1.67	East Siberian Sea	8, 9	[*Shakhova et al.*, 2010]
70	200	3	1.50	Tommeliten, North Sea	7,11	[*Schneider von Deimling et al.*, 2011]
80	50	20	40.00	Storfjorden	8	[*Damm et al.*, 2008]
100	50	25	50.00	Storfjorden	8	[*Damm et al.*, 2008]
125	70	35	50.00	Storfjorden	3	[*Damm et al.*, 2007]
150	80	9	11.25	West Svalbard shelf and inner fjords on the west	7, 9	[*Damm et al.*, 2005]
150	300	8	2.6	West Svalbard PKF slope	6, 7	[*Myhre et al.*, 2016]
200	120	7	5.83	West Svalbard shelf and inner fjords on the west	7, 9	[*Damm et al.*, 2005]
200	40	10	25.00	West Svalbard shelf and inner fjords on the west	7, 9	[*Damm et al.*, 2005]
240	500	4	0.80	PKF slope	8	[*Gentz et al.*, 2014]
360	40	2	5.00	Craters, Barents Sea		[*Lammers et al.*, 1995]
400	120	9	7.50	PKF slope	8	[*Steinle et al.*, 2015]
400	500	3	0.60	PKF slope	7, 8	[*Graves et al.*, 2015]